LES OF TURBULENT SURFACE SHEAR STRESS AND PRESSURE GRADIENT DRIVEN FLOW ON SHALLOW CONTINENTAL SHELVES.

Guillaume Martinat
Coastal Physical Oceanography
Old Dominion University
Norfolk VA
martinat@ccpo.odu.edu

Andres E. Tejada-Martínez
Civil & Environmental Engineering
University of South Florida
Tampa, FL.
aetejada@usf.edu

Chester E. Grosch
Coastal Physical Oceanography
Old Dominion University
Norfolk VA
enright@ccpo.odu.edu

ABSTRACT

Turbulent shear flows on shallow continental shelves are of great importance because tides and wind driven flows on the shelf are drivers of the transfer of momentum, heat, and mass (gas) across the air-sea interface. These turbulent flows play an important role in vertical mixing and transport of sediment and bioactive material. Large Eddy Simulation is used to quantify the effects of pressure gradient and wind shear on the distinctive structures of the flow.

1 Introduction

Turbulence generated by currents, tides and wind driven flows on shallow continental shelves is of importance because of the transfer of momentum, heat, and mass (gas) across the air-sea interface. Understanding the turbulence dynamics of this class of flows presents complications because of the presence of a free surface, the necessity of including the flow interaction with a solid, no-slip bottom and also because the flow can be driven by an imposed pressure gradient for example a tidal current, and/or a wind stress at the free surface or a combination of both. In addition, the presence of a wave field can modify the flow substantially.

The intent of the LES discussed in this paper is to simulate the turbulent flow on shallow shelves having turbulence scales of O(100) m in the horizontal and depths in the range of 10 to 50 m. On these scales the turbulent flow is homogenous in the horizontal. The purpose of our calculations is to elucidate the structure of the turbulence dynamics as driven by pressure gradient driven (tidal) flow and surface stress driven flow without and with waves.

2 Governing Equations

Constant density flow is assumed because we assume that turbulent mixing is strong enough to remove stratification. The equations are solved in non-dimensional form. Let $(\ )^*$ denote a dimensional quantity and $(\ )$ a non-dimensional quantity. The velocity scale is $u^*_{\tau_T} \equiv \sqrt{\tau^*_T/\rho^*}$ with τ^*_T the total stress on the bottom, the length scale $\delta^* = H^*/2$, with H^* the water depth. The non-dimensional vertical coordinate is $-1 \le x_3 \le +1$ with this scaling. The velocity scale used in the non-dimensionalization is $u^*_{\tau_T}$ so the Reynolds number in the non-dimensional equations is Re_{τ_T}.

The Craik-Leibovich (hereafter C-L) equations are derived by applying a time filter to the Navier-Stokes equations (Craik & Leibovich, 1977). Application of a homogeneous, low-pass spatial filter to the non-dimensional C-L equations gives

$$\frac{\partial \overline{u_i}}{\partial x_i} = 0$$

$$\frac{\partial \overline{u_i}}{\partial t} + \overline{u}_j \frac{\partial \overline{u_i}}{\partial x_j} = -\frac{\partial \overline{\Pi}}{\partial x_i} + \frac{1}{Re_{\tau_T}} \frac{\partial^2 \overline{u_i}}{\partial x_j^2} + \frac{\partial \tau_{ij}}{\partial x_j} + \frac{1}{\mathrm{La}_\mathrm{t}^2} \varepsilon_{ijk} U^S_j \overline{\omega}_k + \overline{F}_i \tag{1}$$

where an over-bar denotes application of the low-pass spatial filter and $\overline{u_i}$ and $\overline{\omega}_i$ are the i-th components, in the Cartesian coordinate system (x_1, x_2, x_3), of the non-dimensional space and time filtered velocity and vorticity, respectively, ε_{ijk} is the totally antisymmetric third rank tensor, and $\overline{F_i}$ is the i-th non-dimensional component of the imposed pressure gradient per unit mass. The non-dimensional, modified, space and time filtered pressure is defined as

$$\overline{\Pi} = \overline{p} + \frac{1}{2}\left(\frac{1}{\mathrm{La}_\mathrm{t}^4} U^S_i U^S_i + \frac{2}{\mathrm{La}_\mathrm{t}^2} \overline{u}_i U^S_i\right). \tag{2}$$

where $\overline{p}$ is the non-dimensional pressure.

The fourth (next to last last) term on the right hand side of the second equation in (1) is the non-dimensionalized C-L

vortex force defined as the Stokes drift velocity crossed with the filtered vorticity. The non-dimensional Stokes drift velocity is defined as

$$U_1^s = \frac{\cosh(2\kappa x_3)}{2\sinh^2(\kappa H)} \quad \text{and} \quad U_2^s = U_3^s = 0, \tag{3}$$

where κ is the wavenumber of the dominant filtered-out surface gravity wave. Here we only consider the dominant wave, defined as that of the peak of the wave spectrum, but equation (3) could be generalized to a wave spectrum by integrating the product of the spectral density function and (3) over the wave number spectrum.

The turbulent Langmuir number is $La_t = (u^*_{\tau_p}/u^*_s)^{1/2}$. The characteristic Stokes drift velocity, u^*_s, is defined as $u^*_s = \omega^* \kappa^* a^{*2}$, where ω^* is the frequency, $\kappa^* = 2\pi/\lambda^*$ is the wavenumber with λ^* the wavelength and a^* is the amplitude of the dominant surface gravity wave. In the LES with the C-L force reported here $La_t = 0.7$ and $\lambda^* = 6H^*$.

The subgrid-scale (SGS) stress τ_{ij} in (1), generated by spatial filtering the C-L equations, is defined as $\tau_{ij} = \overline{u_i}\overline{u_j} - \overline{u_i u_j}$. The term $\overline{u_i u_j}$ gives rise to a closure problem and thus must be parameterized. The deviatoric part of τ_{ij} (i.e. $\tau^d_{ij} \equiv \tau_{ij} - \delta_{ij}\tau_{kk}/3$) is parameterized using the dynamic Smagorinsky closure and the dilatational part (i.e. $\delta_{ij}\tau_{kk}/3$) is added to the modified pressure, $\overline{\Pi}$. The details of the implementation of the dynamic Smagorinsky closure are given in Tejada-Martinez & Grosch (2007) (hereafter TMG07) who also implemented a different closure, the dynamic mixed closure of Morinishi & Vasilev (2001), and studied the effects of varying the SGS and the grid resolution on the results (see Appendix C of TMG07) and found that their results were relatively insensitive to model used in computing the SGS. It should be noted that, in contrast to previous LES of flows with LC such as those of McWilliams, *et al.* (1997), Li, *et al.* (2005) and others, the viscous stress term (inversely proportional to *Re*) has been retained. The viscous stress term has been retained because the present simulations resolve bottom and surface viscous boundary layers where this term plays an important role in the governing dynamics.

2.1 Boundary and Forcing Conditions

As in TMG07, we impose periodicity in the horizontal (x_1 and x_2) directions. Periodicity in x_1 and x_2 implies that the flow is spatially homogeneous over these directions. A no-slip boundary condition and a zero normal flow (in the x_3 direction) condition are both imposed at the bottom, thus $\overline{u}_i(x_1, x_2, -1) = 0 \;\; i = 1,2,3$. Consistent with wave (phase) averaging of the equations there is no deformation of the free surface, thus a zero normal flow condition is imposed at the surface, that is $\overline{u}_3(x_1, x_2, 1) = 0$.

The remaining conditions are the forcing conditions *i.e.* the imposed pressure gradient and the imposed wind stress on the surface. We consider, first, the case in which the flow is driven by an imposed pressure gradient without any surface stress. In this case, without loss of generality, we can have the pressure gradient parallel to the x_1 axis so $\overline{F}_1 \neq 0$ and $\overline{F}_2 \equiv 0$. In order to determine $\overline{F}_1$ we integrate the x_1 component of the momentum equation from $x_3 = -1$ to $x_3 = 1$. This gives, in dimensionless variables, $\left(\frac{\partial \overline{u}_1}{\partial x_3}\right)_{x_3=1} - \left(\frac{\partial \overline{u}_1}{\partial x_3}\right)_{x_3=-1} = -2\, Re_{\tau_P}\, \overline{F}_1$. In this case, with the stress on the surface zero, $\left(\frac{\partial \overline{u}_1}{\partial x_3}\right)_{x_3=1} \equiv 0$ and, with the non-dimensionalization, $\left(\frac{\partial \overline{u}_1}{\partial x_3}\right)_{x_3=-1} = Re_{\tau_P}$ thus $\overline{F}_1 = \frac{1}{2}$. In addition, because the stress on the surface is zero, $\left(\frac{\partial \overline{u}_2}{\partial x_3}\right)_{x_3=1} \equiv 0$.

Next consider the case in which there is an imposed surface shear stress. Without loss of generality we take the wind stress, $\tau^*_W \neq 0$, to be parallel to the x^*_1 axis. There may also be an imposed pressure gradient at some angle to the x^*_1 axis which has components $\partial P^*_o/\partial x^*_i$ for $i = 1,2$. The corresponding stresses associated with the pressure gradient are

$$\tau^*_{P_i} = \left(\frac{\partial P^*_o}{\partial x^*_i}\right) H^*; \;\; i = 1,2.$$

Thus the stress in the x^*_1 direction is $\tau^*_W + \tau^*_{P_1}$ and that in the x^*_2 direction is $\tau^*_{P_2}$. The magnitude of the *total stress*, that due to the wind stress and the pressure gradient, is $\tau^*_T = \sqrt{(\tau^*_W + \tau^*_{P_1})^2 + (\tau^*_{P_2})^2}$. It then follows that the relationship of the "friction velocities" is

$$(u^*_{\tau_T})^2 = \sqrt{((u^*_{\tau_W})^2 + (u^*_{\tau_{P_1}})^2)^2 + ((u^*_{\tau_{P_2}})^2)^2}, \tag{4}$$

and that of the "stress Reynolds numbers" is

$$(Re_{\tau_T})^2 = \sqrt{((Re_{\tau_W})^2 + (Re_{\tau_{P_1}})^2)^2 + ((Re_{\tau_{P_2}})^2)^2}. \tag{5}$$

We set $Re_{\tau_T} = 395$ and chose the other terms so that 5 is satisfied. We consider cases in which (a) the wind stress is dominant ($Re_{\tau_W} = 390$ and $Re_{\tau_{P_2}} = 180$) , (b) the pressure gradient stress is dominant ($Re_{\tau_W} = Re_{\tau_{P_2}} = 279$) and (c) the wind stress and pressure gradient stresses are equal ($Re_{\tau_W} = 180$ and $Re_{\tau_{P_2}} = 390$).

2.2 Numerical Method

The numerical method used to solve the governing equations combines 2^{nd} order fractional time stepping with a hybrid spatial discretization. The spatial discretization is spectral in the x_1 and x_2 directions with 5^{th} and 6^{th} order compact differencing and grid stretching in the x_3 direction. The SGS stress is represented by the the dynamic Smagorinsky closure (Smagorinsky, 1963; Lilly, 1992). The details of the method used to solve the governing equations, including the temporal and spatial discretization, the grid stretching, the finite-difference stencils, the SGS stress and the parallel implementation, is described in detail in Appendices E and F of TMG07 and also in Tejada-Martinez, *et al.* (2009).

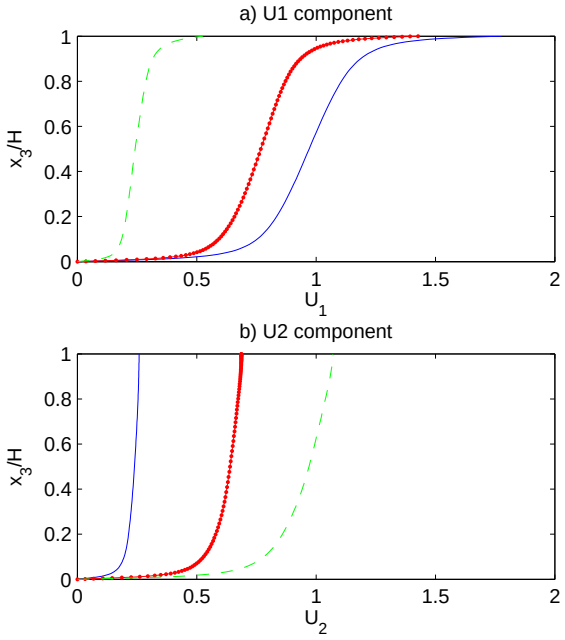

Figure 1. Mean velocity profiles for flows without wave forcing : (a) Streamwise component, (b) Crosstream component. Wind stress dominant in blue, equal wind and pressure gradient stresses in red and Pressure gradient stress dominant in green.

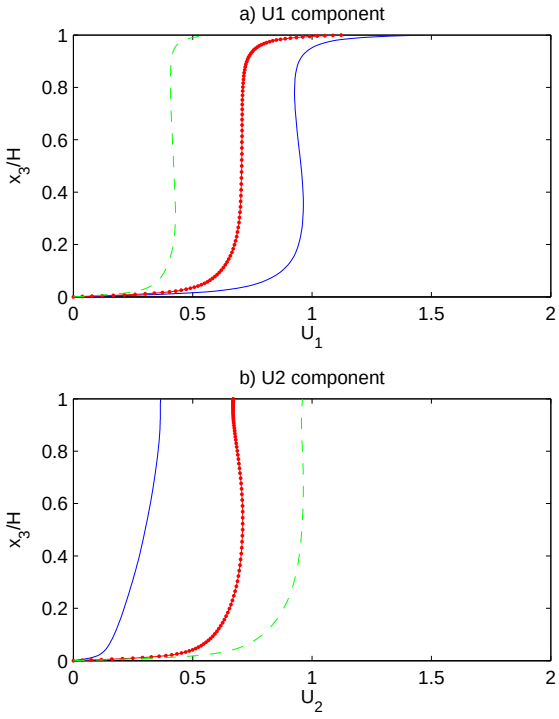

Figure 2. Mean velocity profiles for flows with wave forcing : (a) Streamwise component, (b) Crosstream component. Wind stress dominant in blue, equal wind and pressure gradient stresses in red and pressure gradient stress dominant in green.

3 Results

3.1 Mean profiles and flow visualizations

Figure 1 and 2 show streamwise and cross-stream component mean velocity profiles normalized by the velocity magnitude at midheight for respectively flows without wave forcing and with wave forcing. Without any wave forcing, only the balance of momentum between the pressure gradient flow and the wind driven flow changes. The relative shape of each mean profile stays identical wether the stress is dominant or not.

With wave forcing, we observe major changes in the mean profiles both on streamwise and cross-stram components, all due to the CL forcing. U_1 has a negative slope of the mean profile in the middle of the water column for the wind dominant and pressure gradient dominant cases and is almost constant for the equal stresses case, meaning a more homogeneous flow than without wave forcing. The U_2 component shows very different behaviors : with wind dominant, the mean profile is closer to a laminar pressure gradient driven flow profile than a turbulent one. With equal stresses, the maximum U_2 velocity is located at mid height and the flow is slightly slower at the top of the water column. With a pressure gradient dominant, the U_2 profile is less modified by CL forcing and closer to an unforced pressure gradient mean profile. The maximum U_2 velocity is still located at mid height but the surface velocity is now almost equal to the mid height one.

Figure 3 shows $u_1'/ < u_1 >$ on (x_1, x_2) plane at $x_3 = 0$ (mid height). Mean flow is in the direction of increasing x_1. The tilt of the streaks in the cross-stream direction is due to the cross-stream pressure gradient. The magnitude of the tilt is dependant on the balance between the wind stress and the pressure gradient. The addition of the wave forcing results in a single cell structure, panels (b), (d) and (f), in place of a two cell structure, panels (a) and (c) or no coherent structure at all, panel (e).

3.2 Resolved Reynolds stresses

The normal and shear stresses are shown in figure 4 for cases without wave forcing and figure 5 for cases with wave forcing. For cases with wind dominant, $\langle \overline{u_1' u_1'} \rangle$ is the dominant normal stress both with and without waves. With an increased contribution of the pressure gradient, $\langle \overline{u_1' u_1'} \rangle$ decreases in the entire water column while $\langle \overline{u_2' u_2'} \rangle$ increases near bottom. The result is a reduction of TKE near the surface while it remains unchanged near the bottom.

Shear stresses are much weaker than normal stresses. Due to the cross flow $\langle \overline{u_1' u_2'} \rangle$ becomes non negligible on the bottom thanks to the growth of $\langle \overline{u_2' u_2'} \rangle$ and is the strongest when the contribution of wind stress and pressure gradient on the bottom stress are equal. $\langle \overline{u_1' u_3'} \rangle$ is stronger than $\langle \overline{u_2' u_3'} \rangle$ and symmetrical while wind stress is dominant and slowly decreases as the pressure gradient contribution increases. $\langle \overline{u_2' u_3'} \rangle$ increases only in the bottom of the boundary layer

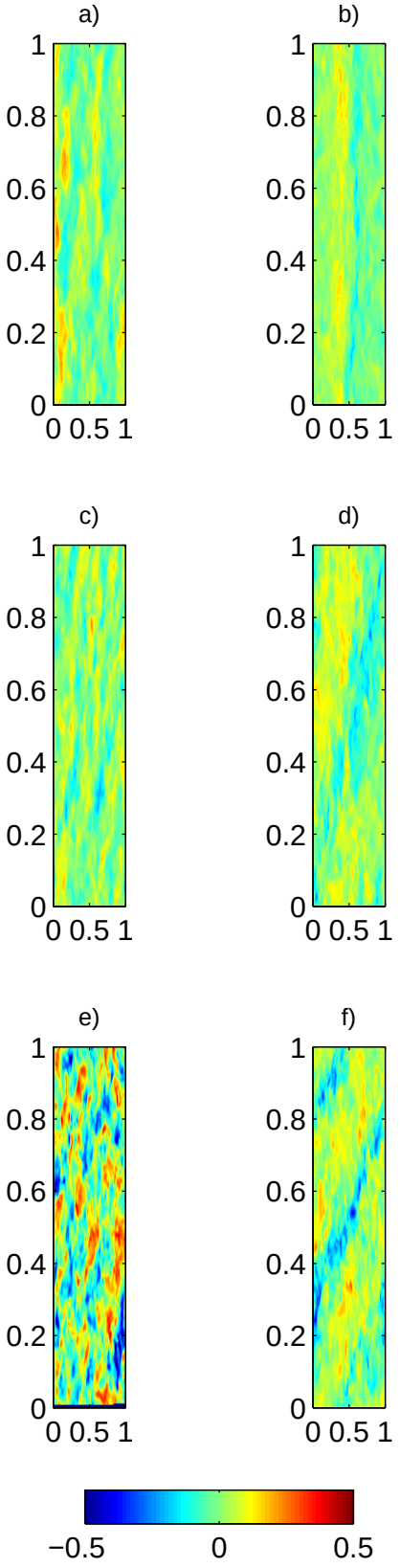

Figure 3. Instantaneous U_1 velocity fluctuationon the x_1x_2 plane at mid height. (a) Wind dominant, (b)Wind dominant with waves , (c) Equal stresses , (d) Equal stresses with waves , (e) Pressure gradient dominant , (f) Pressure gradient dominant with waves

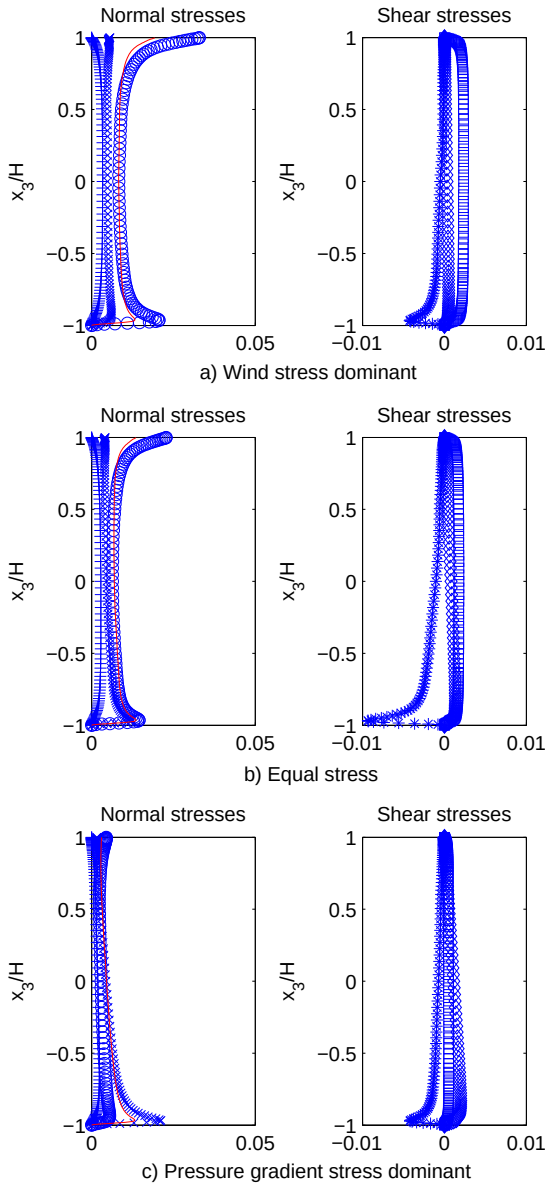

Figure 4. Resolved normal and shear stresses and TKE for flows without wave forcing. The terms are normalized by $(u^*_{\tau_T})^2$. The symbols for the normal stresses are: $\circ$, $\langle\overline{u_1'u_1'}\rangle$; $\times\langle\overline{u_2'u_2'}\rangle$; $+$, $\langle\overline{u_3'u_3'}\rangle$; $-$, TKE. The symbols for the shear stresses are: $*$, $\langle\overline{u_1'u_2'}\rangle$; $\square$,$\langle\overline{u_1'u_3'}\rangle$; $\diamond$, $\langle\overline{u_2'u_3'}\rangle$.

while the pressure gradient contribution to the bottom stress increases.

In every case, the CL forcing increases $\langle\overline{u_1'u_1'}\rangle$ stress. As a consequence for a pressure dominant flow with wave forcing, $\langle\overline{u_1'u_3'}\rangle$ remains high close to the bottom of the water column since both $\langle\overline{u_1'u_1'}\rangle$ and $\langle\overline{u_2'u_2'}\rangle$ are non negligible.

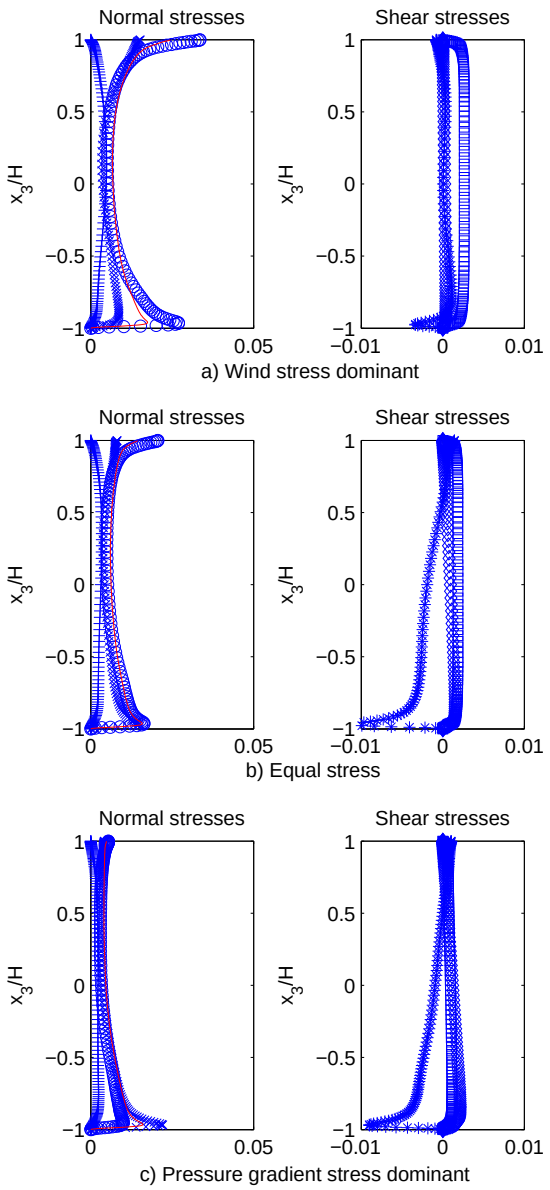

Figure 5. Resolved normal and shear stresses and TKE for flows with wave forcing. The terms are normalized by $(u^*_{\tau_T})^2$. The symbols for the normal stresses are: $\circ$, $\langle\overline{u_1'u_1'}\rangle$; $\times\langle\overline{u_2'u_2'}\rangle$; $+$, $\langle\overline{u_3'u_3'}\rangle$; , TKE. The symbols for the shear stresses are: $*$, $\langle\overline{u_1'u_2'}\rangle$; $\Box$,$\langle\overline{u_1'u_3'}\rangle$; $\diamond$, $\langle\overline{u_2'u_3'}\rangle$.

3.3 Invariants of the Reynolds Stress Anisotropy Tensor

The Reynolds stress anisotropy tensor, b_{ij}, is (Lumley, 1978; Pope, 2001)

$$b_{ij} = \frac{\langle\overline{u_j'u_j'}\rangle}{2} - \frac{1}{3}\delta_{ij}. \quad (6)$$

This is a real, symmetric second order tensor (matrix) with a zero trace. Hence, it has three real eigenvalues of which one or two, but not three, must be negative. The three eigenvalues are invariants of b_{ij}. Three other invariants of b_{ij} are

$$I = b_{ii} = trace(b_{ij}) = 0;\ II = b_{ij}b_{ji};\ III = b_{ij}b_{jk}b_{ki}. \quad (7)$$

The "triangle" of Figure 6 in the $(II^{1/2}, III^{1/3})$ plane is the Lumley triangle (Lumley, 1978; Pope, 2001) and all realizable states of turbulent flow must lie within it. The trajectory begins at the first grid point above the bottom (at $x_3^+ = 1$) in the viscous sublayer. This point is just below the curve of two-component turbulence and in the vicinity of the one-component vertex because, very close to a solid boundary, the magnitudes of $\langle\overline{u_1'u_1'}\rangle$ and $\langle\overline{u_2'u_2'}\rangle$ are much larger than that of $\langle\overline{u_3'u_3'}\rangle$. Moving away from the bottom boundary the trajectories in all cases move parallel to the two-component side towards the one-component vertex as $\langle\overline{u_1'u_1'}\rangle$ increases relative to the other two. A short distance above the bottom ($x_3^+ \approx 7$) at the top of the viscous sublayer reverse direction and move away from the one-component vertex. This structure of the trajectory is characteristic of all turbulent shear flows very close to a solid boundary. Above the near wall region, the invariant trajectory is sensitive to the structure of the particular flow.

The wind dominant and equal stress cases, both with no wave, have a trajectory that is characteristic of a flow with boundary layers at both the surface and the bottom with substansial symmetry of the normal stresses about mid-depth. Because of the symmetry, the trajectory in the upper half is almost identical to the one in the lower half. The wind dominant and equal stress cases both with wave have a different trajectory. After reversing direction at the top of the viscous sublayer, the trajectory moves parallel to and just below the two-component side of the triangle towards the two-component isotropic vertex. This occurs because the C-L vortex drives $\langle\overline{u_2'u_2'}\rangle$ comparable to $\langle\overline{u_1'u_1'}\rangle$ in the upper third of the water column. In the center of the water column $\langle\overline{u_2'u_2'}\rangle$ is smaller than the other two terms so the trajectory crosses the triangle and is parallel to the axi-symmetric side in the region of mid-depth and then moves back across the triangle below mid-depth. In the upper third of water column the trajectory is three-component for a distance, switches to axi-symmetric and then to two-component as $\langle\overline{u_3'u_3'}\rangle \rightarrow 0$ at the upper surface with the other two stresses becoming larger.

The pressure dominant trajectory with no wave forcing is similar to the one of wind stress dominant until mid-height of the water column where the trajectory moves towards a disk shaped turbulence before coming back to a dominantly one component turbulence. This occurs because around mid height, though dominant on the bottom, $\langle\overline{u_2'u_2'}\rangle$ is of the same order of magnitude as $\langle\overline{u_1'u_1'}\rangle$, hence the two component turbulence. However, since it is predominantly created by the pressure gradient stress $\langle\overline{u_2'u_2'}\rangle$ is close to 0 at the surface where the wind stress and $\langle\overline{u_1'u_1'}\rangle$ despite their small magnitude are dominant inducing a predominantly one component turbulence.

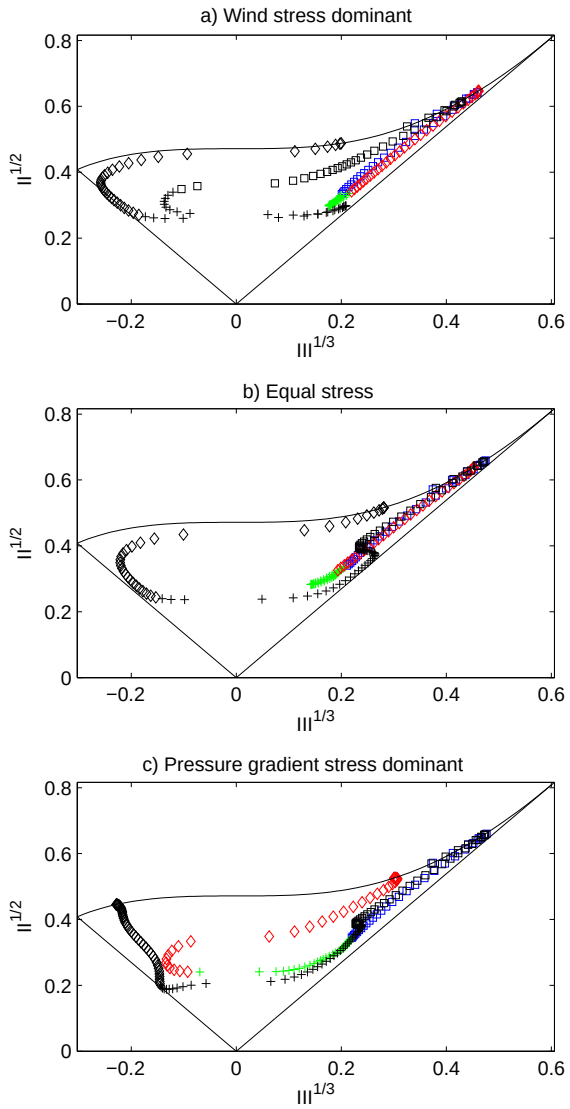

Figure 6. Trajectory as a function of the distance from the bottom of the invariants of b_{ij} in the $(II^{1/2}, III^{1/3})$ plane for the three cases of for wind stress dominant flows without waves (color) and with waves (black). □ :-1 ¡ $x_3 < -0.5$, $+ : -0.5 < x_3 < 0.5$, ⋄ :0.5 ¡ $x_3 < 1$

The pressure dominant trajectory with wave forcing is similar to the one without wave forcing until the upper part of the boundary layer where it remains close to the 2 component vertex. This can be explained by the increase of $\langle \overline{u_2' u_2'} \rangle$ to the same order of magnitude as $\langle \overline{u_1' u_1'} \rangle$ by CL forcing.

4 Conclusion

Though the dynamics of a surface stress driven and a pressure gradient driven flow are different, without wave forcing, the balance between their stress does not impact significantly the flow structure. In contrast, CL vortex force has a significant impact, homogeneizing the flow and forcing a negative slope on U_1 mean profile near the middle of the water column and U_2 in its upper part. This has important consequences for turbulence parametrization since numerous models use a turbulent eddy viscosity concept where the Reynolds stress anisotropy tensor a_{ij} is modeled as $a_{ij} = -2\nu_t \overline{S_{ij}}$. In its simplest form, it reduces to respectively $\langle \vec{u_1'} \vec{u_3'} \rangle = -\nu_t \frac{\partial u_1}{\partial x_3}$ and $\langle \vec{u_1'} \vec{u_2'} \rangle = -\nu_t \frac{\partial u_1}{\partial x_2}$. With $\frac{\partial u_1}{\partial x_3}$ and $\frac{\partial u_1}{\partial x_2}$ negative and ν_t positive, this simple parametrization gives positive Reynolds stresses where negative stresses are oberved. Finally, the trajectory of the invariant of the Reynolds stress anisotropy tensor has been seen to be a sensitive indicator of the structure of turbulence. When wave-current driven Langmuir circulation is observed, the turbulence as a much more three-component structure than when it is not.

Aknowledgements

The support of the National Science Foundation through Grant 0927724 and of Teragrid through Project OCE-100008 is gratefully acknowledged.

REFERENCES

Craik, A.D.D. & Leibovich, S. A rational model for Langmuir circulation. *J. Fluid Mech.* **73**, 401-426, 1976.

Li, M., Garret, C. & Skyllingstad, E. A regime diagram for classifying turbulent large eddies in the upper ocean. *Deep Sea Res. I* **52**, 259-278, 2005.

Lilly, D.K. A proposed modification of the Germano subgrid-scale closure. *Phys. Fluids* **3**, 2746-2757, 1992.

Lumley, J.L. Computational modeling of turbulent flows. In *Advan. App. Mech.*, **18**, 123-176, 1978.

McWilliams, J.C., Sullivan, P.P. & Moeng, C.-H. Langmuir turbulence in the ocean. *J. Fluid Mech.* **334**, 1-30, 1997.

Morinishi, Y. & Vasilev, O.V. A recommended modification to the dynamic two-parameter mixed subgrid scale model for large eddy simulations of turbulent flows. *Phys. Fluids* **13**, 3400-3410, 2001.

Pope, S.B. *Turbulent Flows.* Cambridge University Press, 2001.

Smagorinsky, J. General circulation experiments with the primitive equations. I. The basic experiment. *Mon. Wea. Rev.* **91**, 99-164, 1963.

Tejada-Martínez, A. E. & Grosch, C.E. "Langmuir turbulence in shallow water. Part 2. Large-eddy simulation", *J. Fluid Mech.* **576**, *63-108, 2007.*

Tejada-Martínez, A. E. & Grosch, C.E. Gargett, A.E., Polton, J.A., Smith, J.A., & MacKinnon, J.A. "A hybrid spectral/finite-difference large-eddy simulator of turbulent processes in the upper ocean", *Ocean Modeling, 30, 115-142, 2009.*